BIOCHEMISTRY
including biophysical chemistry & molecular biology

Accelerated Publication

pubs.acs.org/biochemistry

The Tyrosine Gate as a Potential Entropic Lever in the Receptor-Binding Site of the Bacterial Adhesin FimH

Adinda Wellens,[†] Martina Lahmann,[‡] Mohamed Touaibia,[∥,§] Jonathan Vaucher,[∥] Stefan Oscarson,[⊥] René Roy,*[,∥] Han Remaut,[†] and Julie Bouckaert*[,†,@]

[†]Structural Molecular Microbiology, Vrije Universiteit Brussel, VIB, Brussels, Belgium

[‡]School of Chemistry, Bangor University, Bangor LL57 2UW, United Kingdom

[§]Department of Chemistry and Biochemistry, Université de Moncton, Moncton, New Brunswick, Canada E1A 3E9

[∥]Department of Chemistry, Université du Québec à Montréal, Montreal, Québec, Canada

[⊥]Centre for Synthesis and Chemical Biology, University College Dublin, Belfield, Dublin 4, Ireland

[@]Unité de Glycobiologie Structurale et Fonctionnelle, UMR 8576 du CNRS, Villeneuve d'Ascq, France

Supporting Information

ABSTRACT: Uropathogenic *Escherichia coli* (UPEC) are the major causative agents of urinary tract infections. During infection, UPEC adhere to mannosylated glycoreceptors on the urothelium via the FimH adhesin located at the tip of type 1 pili. Synthetic FimH antiadhesives such as alkyl and phenyl α-D-mannopyranosides are thus ideal candidates for the chemical interception of this crucial step in pathogenesis. The crystal structures of the FimH lectin domain in its ligand-free form and in complexes with eight medium- and high-affinity mannopyranoside inhibitors are presented. The thermodynamic profiles of the FimH−inhibitor interactions indicate that the binding of FimH to α-D-mannopyranose is enthalpy-driven and has a negative entropic change. Addition of a hydrophobic aglycon influences the binding enthalpy and can induce a favorable entropic change. The alleviation of the entropic cost is at least in part explained by increased dynamics in the tyrosine gate (Tyr48 and Tyr137) of the FimH receptor-binding site upon binding of the ligand. Ligands with a phenyl group directly linked to the anomeric oxygen of α-D-mannose introduce the largest dynamics into the Tyr48 side chain, because conjugation with the anomeric oxygen of α-D-mannose forces the aromatic aglycon into a conformation that comes into close contact (≈2.65 Å) with Tyr48. A propargyl group in this position predetermines the orientation of the aglycon and significantly decreases affinity. FimH has the highest affinity for α-D-mannopyranosides substituted with hydrophobic aglycons that are compatible in shape and electrostatic properties to the tyrosine gate, such as heptyl α-D-mannose.

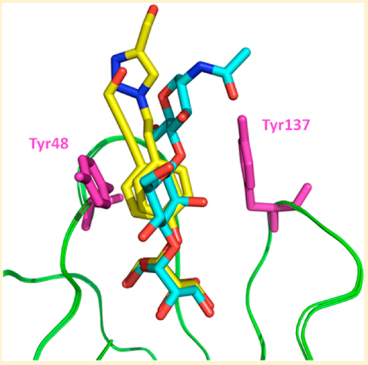

Urinary tract infections (UTIs) are some of the most common bacterial infections.[1] Half of the female population will experience at least one UTI in their lives. In 20−30% of the cases, UTI symptoms recur two or more times within months of a primary infection, and up to one of 20 patients even suffers from chronic forms of UTIs. Although they are usually treated well with available antibiotics, the recurrent character of UTIs and the increased multidrug resistance of uropathogenic *Escherichia coli* (UPEC) make the search for alternative and more efficient approaches imperative. Prophylactic agents are needed to counter the high share of UTIs among hospital-acquired infections (UTIs make up 20 to 40% of nosocomial infections), particularly in catheterized patients.

Pili are prominent virulence factors mediating adhesion of pathogenic bacteria to host cell receptors. Bacterial adhesion is an initial and critical step in pathogenesis, allowing host recognition and preventing bacteria from being washed out by the host. The principal instigator of UTIs is UPEC, which expose mannose-sensitive type 1 pili on their outer surface.[2] Type 1 pili are heteropolymeric fibers that carry a two-domain adhesin, FimH, at their distal tip. FimH adheres via its lectin domain (LD) to terminal mannopyranose units of uroplakin Ia and $\alpha_3\beta_1$ integrins, membrane glycoproteins that are abundantly expressed on superficial epithelial cells of the urinary tract.[3,4]

Upon adhesion, a small percentage of bacteria invade the urothelial cells. Invading bacteria replicate and mature into dense, intracellular bacterial communities (IBC) with biofilm-like properties in preparation for breaking out and infecting neighboring cells.[5] In addition, a number of the internalized bacteria in the subepithelial tissue go into a quiescent state.[6] In most cases, the bacteria associated with a recurrent UTI are clonal with the strain of the initial acute infection, and thus, bacteria recruited from those quiescent intracellular reservoirs are the major cause of recurrent UTIs.[7]

Received: February 24, 2012
Revised: May 28, 2012
Published: June 1, 2012

dx.doi.org/10.1021/bi300251r | *Biochemistry* 2012, 51, 4790−4799

Table 1. Thermodynamic Signature of FimH−Mannoside Derivative Binding

compd	n	ΔH (kcal/mol)	$T\Delta S$ (kcal/mol)	ΔG (kcal/mol)	K_d (nM)
		Alkyl α-D-Mannosides			
HM	0.817 ± 0.003	−13.64 ± 0.10	−2.65	−11.00	7.3 ± 1.8
2	0.932 ± 0.004	−9.78 ± 0.07	0.52	−10.30	23.6 ± 3.6
3	0.933 ± 0.009	−9.70 ± 0.17	0.43	−10.14	31.2 ± 8.8
1	0.828 ± 0.004	−11.34 ± 0.08	−1.58	−9.75	59.5 ± 4.7
BM	0.869 ± 0.006	−9.73 ± 0.10	−0.53	−9.20	153.6 ± 16.1
MM	0.875 ± 0.002	−9.88 ± 0.03	−1.89	−8.01	1197.6 ± 36.9
		α-D-Mannose			
Man	0.773 ± 0.004	−13.64 ± 0.10	−5.84	−7.80	1672.2 ± 94.5
		Aryl α-D-Mannosides			
4	0.891 ± 0.007	−8.55 ± 0.14	2.00	−10.55	18.3 ± 5.9
5	1.190 ± 0.007	−10.01 ± 0.10	0.03	−10.05	36.5 ± 6.4
8	1.050 ± 0.005	−11.08 ± 0.10	−1.34	−9.74	61.0 ± 9.6
7	0.933 ± 0.009	−6.70 ± 0.01	2.80	−9.50	94.3 ± 18.1
6	1.160 ± 0.012	−9.45 ± 0.15	−0.02	−9.43	104.6 ± 21.9

Type 1 pili are essential in pathogenesis, primarily in the adhesion of bacteria to bladder cells, followed by the colonization and invasion of the urothelium, but also in IBC formation and recurrent or chronic UTIs.[8] Early studies have shown that small compounds can hamper UPEC in different stages of their pathogenic cascade.[9] Type 1 pili and the FimH adhesin therefore present an attractive target for the design of antibacterial agents.[10,11]

Mannosides with an apolar substituent have been found to mimic the interactions of high-mannose glycans with the FimH receptor-binding site[12,13] and are known as good inhibitors of UPEC adhesion.[10,14,15] Following this lead, we have generated a set of α-D-mannopyranosides carrying alkyl and aryl moieties. A crystal structure of the FimH lectin domain in its ligand-free form was determined at high resolution, and structures with the eight inhibitors are presented. In cocrystal structures, the electron density is very well-defined both for the α-D-mannoside and for the aglycon, but Tyr48 is almost systematically engaged in lattice contacts between unit cells. Soaking of the ligands into ligand-free crystals of FimH confirmed a dynamic Tyr48 aromatic side chain, in agreement with the finding of several discrete conformers of Tyr48 in the cocrystal structures. Increased dynamics in the binding site of FimH in complex with our soaked-in ligands made the aglycon structure less well-defined by the electron density. To supplement the crystallographic data, we measured enthalpic and entropic contributions of the FimH−ligand interactions using isothermal titration calorimetry (ITC).[16]

EXPERIMENTAL PROCEDURES

Protein Expression and Purification. The FimH lectin domain (LD, residues 1−158) of UPEC strain J96 was expressed and purified as previously described.[10]

Mannopyranosides. Peracetylated mannopyranose reacted with methyl 9-hydroxynonanoate to provide **2** after deacetylation with NaOMe in methanol.[17] The methyl ester was hydrolyzed with NaOH in a water/methanol mixture to produce **3**.[18] The series of *O*-mannosides **1** and **4**−**8** were synthesized as necessary using Sonogashira and Heck cross couplings as well as click chemistry, with a focus on specific aglycon moieties (J. Vaucher, Masters Thesis, 2007, Université du Québec à Montréal, Montreal, QC).

Crystallization and Data Collection. Crystallization of apo FimH LD was screened by hanging-drop vapor diffusion using Hampton Research Crystal Screens 1 and 2. Needle-shaped crystals were obtained at 293 K in 1 M Li_2SO_4, 100 mM Tris (pH 8.6), 10 mM $NiCl_2$, and 0.2 M nondetergent sulfobetaine 201 in space group $P3_121$. The crystals were flash-cooled to 100 K in the precipitant solution complemented with 20% ethylene glycol, as a cryoprotectant. Apo FimH LD crystals were soaked overnight with the mannoside derivatives, yielding FimH complexes in the trigonal crystals. Data for crystals soaked with ligands **1**, **2**, **5** and **7** have been collected on Proxima 1 (SOLEIL, Saint-Aubin, France) and on ID23-2 (ESRF, Grenoble, France) after the crystals had been flash-frozen by the addition of 20% glycerol as a cryoprotectant. Cocrystals have been set up using a 2:1 molar ratio of compound to FimH LD. Drops composed of equal volumes of sample and precipitant solution with 30% (v/v) 2-propanol, 100 mM Tris-HCl (pH 8.5), and 200 mM ammonium acetate for FimH−**7** and 2% PEG8000 and 0.5 M Li_2SO_4 for FimH−**8** were subjected to the sitting drop vapor diffusion method at 293 K. Small needlelike crystals of ∼10 Å × 10 Å × 500 Å were obtained and flash-cooled to 100 K in the precipitant solution with 20% glycerol added as cryoprotectant. X-ray data were collected at 100 K at Proxima 1 to resolutions of 1.9 Å for FimH−**7** and 1.4 Å for FimH−**8**.

Structure Determination and Refinement. Data have been indexed, processed, and scaled using the XDS package.[19] Initial phases have been obtained by molecular replacement with PHASER using a monomer of FimH LD [chain A of Protein Data Bank (PDB) entry 2VCO] as a search model.[20] The resulting molecular replacement solution was submitted to restrained refinement using Refmac 5.2,[21] with 5% of the data retained for cross-validation purposes. Maximum likelihood restrained refinement was combined with manual model adjustment and electron density inspection performed in Coot graphics.[22] Geometric restraints for all ligands were generated using Elbow from the Phenix suite.[23] The ligand's position and conformation were further optimized by running several cycles of successive maximum likelihood restrained refinement using Phenix.[24] For parts of the aglycon with poorly defined electrons, the aglycon was placed to conform to the geometric restraints of the geometric library file and its position was corrected according to the difference electron densities upon refinement. B factors were normalized via the equation $B_{norm} = (B - B_{mean})/\sigma$, where B is the atomic displacement parameter as reported in the PDB entry and B_{mean} the mean

dx.doi.org/10.1021/bi300251r | Biochemistry 2012, 51, 4790−4799

Chart 1. Novel Synthetic Monovalent Mannopyranose Derivatives as FimH Antagonists

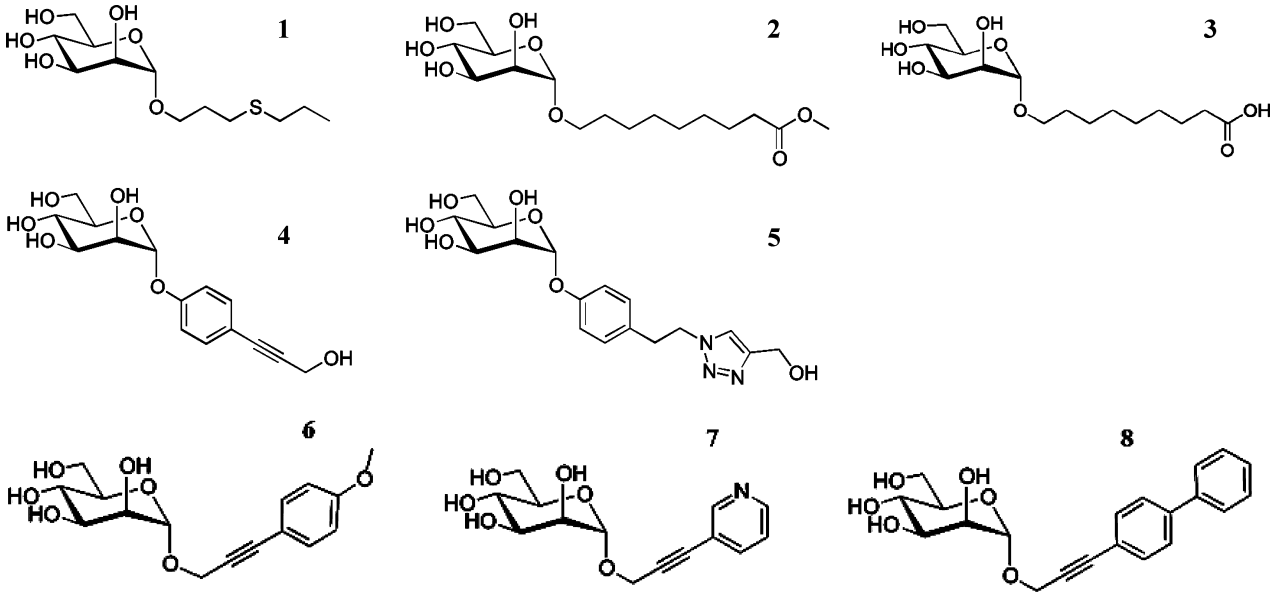

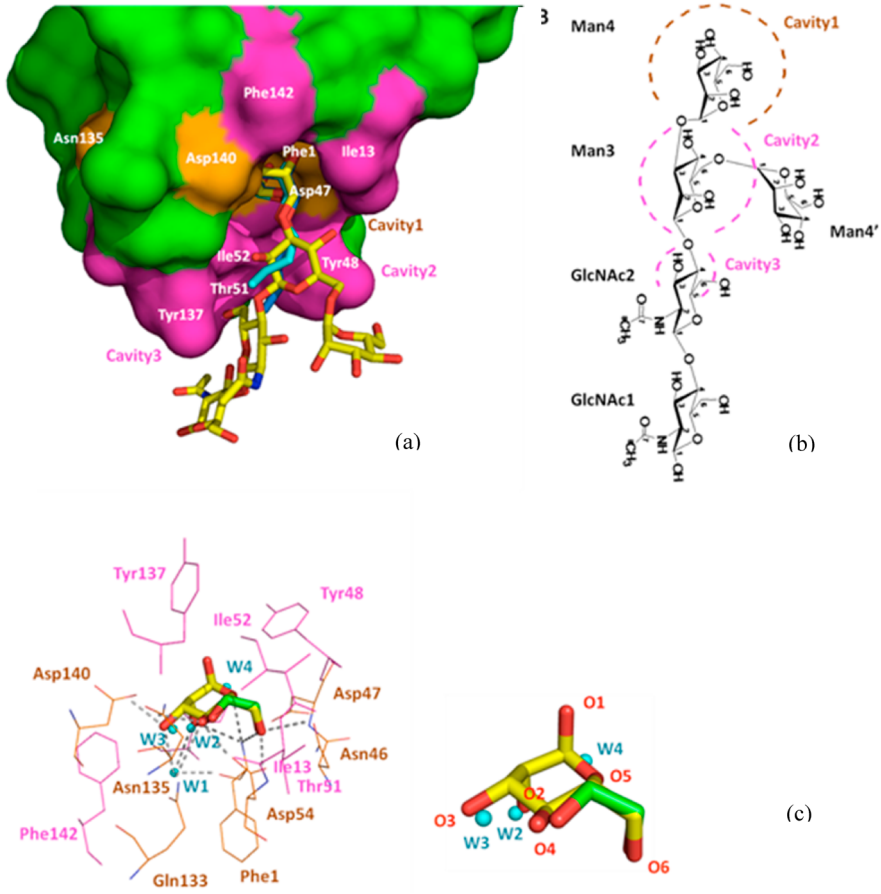

Figure 1. Receptor-binding site of FimH. (a) Surface of the lectin domain of FimH in complex with oligomannose-3 (PDB entry 2VCO, yellow) and butyl α-D-mannopyranoside (PDB entry 1UWF, blue, and PDB entry 1TR7, cyan). A polar mannose-binding pocket forms cavity 1 (orange) and is followed by a hydrophobic groove or cavity 2 and 3 (magenta) interacting with the B face of the central mannose and with the chitobiose core. (b) Schematic representation of the receptor-binding site of FimH bound to oligomannose-3. Cavity 1 is involved in interactions with Man4, cavity 2 with Man3, and cavity 3 with GlcNAc2 and the β1,4 link between Man3 and GlcNAc2. (c) Ethylene glycol (green) and three water molecules (W2–W4, cyan spheres) bound in the receptor-binding site of the apo FimH LD closely mimic hydroxyls O2, O3, and O5 of α-D-mannopyranose (yellow). Residues (orange) that make polar interactions (gray dotted lines) with either mannose or ethylene glycol and the water network (cyan spheres) are shown.

dx.doi.org/10.1021/bi300251r | *Biochemistry* 2012, 51, 4790–4799

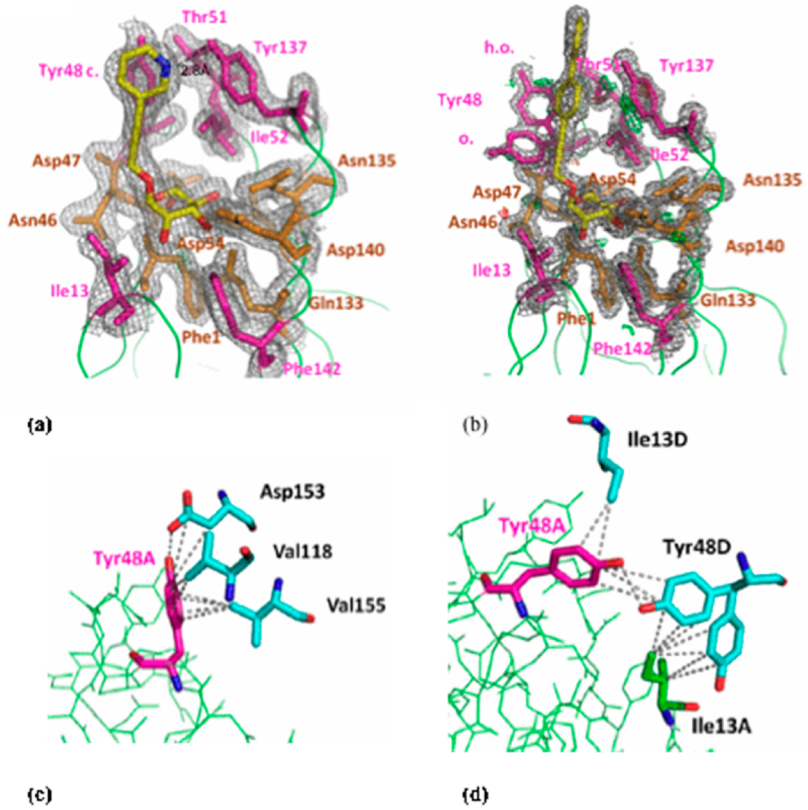

Figure 2. Cocrystal structures of FimH with **7** or **8** show the conserved position of the mannopyranoside (yellow). The apolar aglycon tail is involved in van der Waals contacts with the hydrophobic groove (magenta sticks). (a) FimH−**7** interactions with electron density at 1σ for $2F_o - F_c$ (gray) and 3σ for $F_o - F_c$ (green). (b) In FimH−**8** cocrystals, the Tyr48 side chain is found in two alternate, open (o.) and half-open (h.o.) conformations in molecules B−D of the asymmetric unit. (c) Tyr48 is involved in lattice contacts in orthorhombic space group $P2_12_12_1$ of the FimH−**7** crystals. The crystal packing keeps Tyr48 (magenta) in the closed (c.) conformation. (d) In the triclinic FimH−**8** cocrystals, four molecules are present in the asymmetric unit. Tyr48 (magenta) of molecule A is in the open conformation and makes contacts with Ile13 and Tyr48 that take open and half-open conformations of molecule D (cyan).

and σ the standard deviation of the *B* factors for all C_α atoms in a given protein structure.[25] The residues of the receptor-binding pocket and the ligand are colored by the normalized *B* factors using PyMol version 0.99.

Isothermal Titration Calorimetry. ITC measurements were taken using a VP-ITC (Microcal). Prior to the measurement, the FimH was dialyzed to 20 mM Hepes (pH 7.4) and 150 mM NaCl and the carbohydrates were diluted in this same buffer. Injections of 10 μL of ligand (86 μM to 1.19 mM) were added at 240−1000 s intervals from a computer-controlled 250 μL syringe to the FimH LD solution (9−77 μM) that was being constantly stirred at 307 rpm and 295.15 K. The experimental data were fit with Microcal's Origin 7.0 to obtain the dissociation equilibrium constant K_d, the binding enthalpy ΔH, and the molar ratio *n*. Compound **8** had a >1 molar ratio in the initial measurements using the dialysis buffer. To render **8** completely soluble, as evaluated by *n* converging to 1, we added 10% dimethyl sulfoxide. Calorimetric measurements were repeated in at least two independent experiments to evaluate the consistency between measurements and protein batches. The measured and calculated values for the experiment with the best fit to the model are reported in Table 1.

RESULTS

To establish a detailed interaction profile and to rationalize binding affinities of FimH with medium- and high-affinity binders, we present the crystal structures and thermodynamic signatures[26] of a small and targeted series of FimH antagonists (Chart 1). Two types of FimH inhibitors were probed: α-D-mannosides linked to an alkyl chain intended to mimic the known heptyl α-D-mannoside inhibitor (ligands **1**−**3**) with an internal sulfur (**1**), terminal methyl ester (**2**), or terminal carboxylic acid (**3**) and α-D-mannosides containing an aryl group that may have favorable aromatic stacking interactions within the tyrosine gate of the lectin (ligands **4**−**8**). Prior to the analyses of changes in the FimH receptor-binding site induced by the binding of particular ligands (Chart 1), we determined the structure of the ligand-free (apo) FimH lectin domain.

Crystal Structure of the Mannopyranoside-Free FimH Lectin Domain. Crystal structures have shown that the FimH receptor-binding site consists of a defined polar mannopyranose-binding pocket (Phe1, Asn46, Asp47, Asp54, Gln133, Asn135, and Asp140) and a surrounding hydrophobic ridge (Ile13, Tyr48, Ile52, Tyr137, and Phe142).[27] On the basis of the crystal structures of FimH in complex with butyl α-D-mannopyranoside, and with its minimal oligomannose glycan receptor, oligomannose-3, the binding site of FimH can be subdivided into two major subsites and one minor subsite (Figure 1a,b).[10,11] Cavity 1 also recognizes the α1,3-linked mannose at a nonreducing end of oligomannose-3 with an elaborated hydrogen bond network and encloses the α-D-mannopyranose moiety of alkyl and aryl mannopyranosides.[11,13] Cavity 2 makes mainly apolar contacts with the alkyl aglycon or the central mannose in oligomannoside-3, by

dx.doi.org/10.1021/bi300251r | *Biochemistry* 2012, 51, 4790−4799

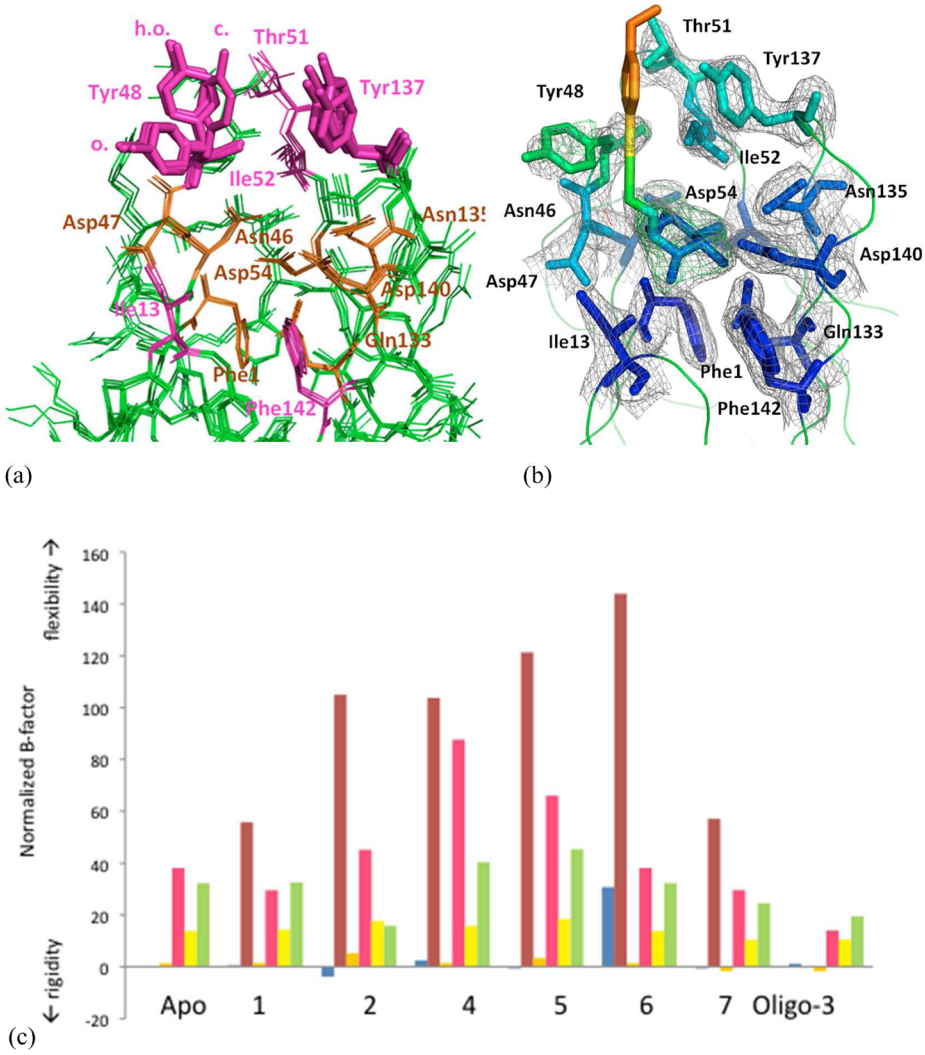

Figure 3. Conformational freedom in the binding pocket of FimH upon the binding of mannopyranosides. (a) The residues of the polar mannose-binding pocket (orange) are strongly engaged in binding the mannopyranose ring, whereas the side chain of Tyr48 (magenta) shows flexibility. Tyr48 is found in three different rotamer conformations, which create an open (o.), half-open (h.o.), or closed (c.) tyrosine gate together with Tyr137 in FimH. (b) Receptor-binding site of apo FimH crystals soaked with inhibitor **6**. The colors range from dark blue for the most rigid atoms to dark red for highly flexible atoms. The electron density is displayed at the 1σ level (gray). (c) Plot of the flexibility of the FimH binding site residue and inhibitors in the crystal structures (Oligo-3 from PDB entry 2VCO). The dynamic behaviors of mannose (blue), the pocket (orange), the ligand aglycon (brown), Tyr48 (magenta), Ile52 (yellow), and Tyr137 (green) are measured in terms of B_{norm}.

residues Tyr48 and Ile52. Cavity 3 formed by Thr51 and Tyr137 side chains accommodates the *N*-acetyl β-D-glucosamines linking the mannotriose core of the oligomannoside to a recognized glycoprotein receptor for FimH. Together, Tyr48 and Tyr137 are lining the hydrophobic groove of the binding site and create the so-called tyrosine gate (Figure 1a).[11]

Crystallization screens of the lectin domain of the fimbrial FimH adhesin in its mannopyranoside-free form resulted in needlelike or rod-shaped crystals, which diffracted to a resolution of 1.5 Å. The crystals contain two molecules in the asymmetric unit and are in primitive trigonal space group $P3_121$ with the following unit cell dimensions: a = 90.9 Å, b = 90.9 Å, and c = 79.8 Å (Table S1 of the Supporting Information).

In the apo FimH structure, the mannose-binding pocket or cavity 1 contains an ethylene glycol molecule that was used as a cryoprotectant. Ethylene glycol in the receptor-binding site of FimH follows the O4−C5−C6−O6 trace of mannopyranoside (Figure 1c, close-up). The diol matches exactly with O4 and O6 of mannose (Figure 1c). Three water molecules, W2−W4, adopt the position and interactions of mannopyranose hydroxyl groups O2, O3, and O5, respectively. The strictly conserved water molecule that hydrogen bonds to O2 and the O of Phe1 is clearly present, too [W1 (Figure 1c)]. The waters and ethylene glycol structurally mimic those polar groups of the mannose that are known to be essential for the interaction within the mannose-binding pocket. It is indeed common that in ligand-free carbohydrate-binding sites, water molecules substitute for the glycan polar groups with the largest hydrogen bonding potential.[28,29] The anomeric O1 is not replaced by a water molecule in the apo FimH structure, in agreement with ligand-bound structures that show that O1 is not involved in direct interactions with the FimH binding pocket.

FimH Cocrystallized with Mannopyranoside Inhibitors Carrying Alkyl and Aryl Moieties in the Aglycon. Crystals of the FimH LD in complex with **7** and **8** were grown and their structures determined to 1.9 and 1.4 Å resolution, respectively (Chart 1). The obtained cocrystals with **7** contain a single FimH LD−inhibitor molecule per asymmetric unit in

dx.doi.org/10.1021/bi300251r | *Biochemistry* 2012, 51, 4790−4799

orthorhombic space group $P2_12_12_1$. Cocrystals of FimH LD in complex with **8** belong to the primitive triclinic space group ($P1$) comprising four molecules in the asymmetric unit. The cocrystal structures each showed well-defined electron density for ligand **7** or **8** bound to the receptor-binding site of FimH. As expected, the mannopyranose moiety of the inhibitors binds tightly with the residues comprising the deep binding pocket at cavity 1, whereas the apolar aglycon of the mannopyranosides occupies cavities 2 and 3, interacting with Thr51 and Ile52, and establishes aromatic stacking interactions with the tyrosine gate of FimH (Figure 2a,b). Superimposing the FimH LD of these two FimH−inhibitor complexes demonstrates that the tyrosines gate exhibits plasticity, whereas the polar mannose-binding residues in the pocket remain relatively rigid (Figure 3a). In particular, Tyr48 and Tyr137, which embrace the aglycon, exhibit considerable conformational differences between the crystal structures.

Analysis of the apo FimH LD structure shows that, in its resting state, the tyrosine gate is found in the open state: the Tyr48 side chain is positioned inward and toward Asp47 and Arg98 (Figure 1 and Figure S1 of the Supporting Information). In the inhibitor complexes, the Tyr48 side chain either rests in its open conformer [o.] or Tyr48 turns toward Thr51 to close the tyrosine gate [half open or closed, (Figure 3a] in response to the nature of the aglycon. However, Tyr48 is also engaged in crystal contacts in both cocrystals of the FimH−**7** and FimH−**8** complexes (Figure 2c,d). We wanted to determine whether the observed side chain conformations of Tyr48 were rotamers selected for favorable interactions with the aglycons or whether they were simply conformers stabilized by the crystal packing. The trigonal crystals of apo FimH (Table S1 and Figure S1 of the Supporting Information) allow for these crystal packing-independent analyses, as they have neither the mannose-binding pocket nor the tyrosine gate involved in lattice contacts. We subsequently soaked the trigonal crystals of apo FimH with the different ligands (Chart 1), to allow disclosure of the preferred conformations of the tyrosines and of the aglycon moieties of the ligands in the different FimH complexes.

Conformational Flexibility of Tyr48 and the Inhibitors' Apolar Aglycon upon Binding. Trigonal crystals of apo FimH were soaked overnight with compounds **1**−**8**. For the FimH−mannopyranoside complexes with compounds **1**, **2**, and **4**−**8**, difference electron density ($F_o - F_c$) (Table S2 of the Supporting Information) was observed in the FimH mannose-binding pocket (Figure S2 of the Supporting Information). Crystals soaked with compounds **3** and **8** did not diffract better than 3.5 Å. It is possible that these longer ligands interfered with the lattice contacts in the crystal packing of the trigonal crystals, also indicated by the growth of the FimH−**8** complex in space group $P1$. In each of the structures with compounds **1**, **2**, and **4**−**8**, the mannopyranoside moiety is clearly defined inside cavity 1, while varying degrees of residual $F_o - F_c$ density are observed for the aglycon and neighboring side chains in the different complexes. In particular, Tyr48 and Tyr137 demonstrate substantial disorder (Figure 3b and Figure S2 of the Supporting Information).

The normalized B factors (B_{norm}) of the polar pocket of FimH and of the mannoside derivatives confirm that the mannose and the mannose-binding residues are only slightly dynamic (Figure 3c). The most pronounced rigidity is found in the crystal structure of FimH in complex with oligomannose-3, which is the highest-affinity FimH epitope on high-mannose glycans. The ligand aglycons and Tyr48 show substantial disorder. To a lesser extent, Tyr137 also had an increased flexibility. Ile52 that backs up the two tyrosines in cavity 2 was not influenced at all by the binding of the ligand. Noteworthy, in the apo FimH structure, is the fact that the electron density of Tyr48 is clearly defined and Tyr48 is found in the open conformation (Figure S1 of the Supporting Information). The X-ray structure of mannopyranoside-soaked crystals revealed that for ligands **4** and **5**, having an aryl group right after the glycosidic linkage of mannose, the apolar aglycon dislocates Tyr48 from its open conformation observed in the apo FimH and the oligomannoside-bound structure (Figure S2 of the Supporting Information, **4** and **5**). The X-ray data further indicate that alkyl and aryl tails challenge the open conformation of Tyr48 and induce substantial disorder and dynamics in the tyrosine gate (Figure S2 of the Supporting Information). These dynamics potentially increase the entropy term of binding. To analye this, we identified the thermodynamic signatures of interactions of FimH with the different mannopyranose derivatives (Chart 1) and used ITC to determine enthalpic and entropic contributions to FimH binding (Figures S2 and S3 of the Supporting Information).

Thermodynamic Signature for FimH Inhibitors. For comparison, we divided the compounds into two classes: mannosides with alkyl groups in the aglycon (**1**−**3**) and mannosides with aryl groups in the aglycon (**4**−**8**) (Chart 1, Table 1, and Figures S2 and S3 of the Supporting Information). In addition, the thermodynamic signatures for binding of FimH to D-mannose (Man) and methyl (MM), butyl (BM), and heptyl (HM) α-D-mannopyranosides have been determined. The ITC data revealed that the binding is predominantly enthalpy-driven and that increases in entropy generally compensate for lower enthalpies (Table 1).

A general trend in the ITC data for the class of alkyl mannopyranosides (Figure S3 of the Supporting Information) is that the entropy contribution becomes more positive with an increase in chain length (Figure 4, left-hand side). While D-

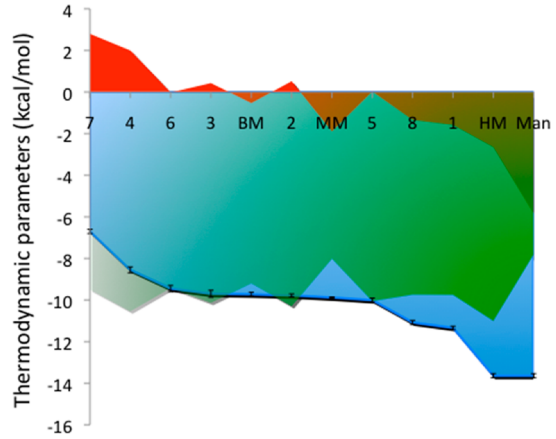

Figure 4. Thermodynamic signatures of FimH−mannoside derivative (along x) interactions, plotted from lower (left) to higher (right) enthalpy to demonstrate the observed enthalpy−entropy compensation. The enthalpy (ΔH, blue), entropy ($T\Delta S$, red), and Gibbs free energy (ΔG, green) are expressed in kilocalories per mole along y. The standard deviations are indicated by small bars.

mannopyranose (K_d = 1.7 μM, or ΔG = −7.80 kcal/mol), methyl α-D-mannopyranoside (K_d = 1.2 μM, or ΔG = −8.01 kcal/mol), and butyl α-D-mannopyranoside (K_d = 154 nM, or

dx.doi.org/10.1021/bi300251r | Biochemistry 2012, 51, 4790−4799

ΔG = −9.20 kcal/mol) still pay an entropic penalty upon binding with FimH, compounds **1**−**3** (K_d of ≤24 nM or ΔG of −10.30 kcal/mol for **2**) gain Gibbs free energy with a constructive entropic contribution. The only exception is HM, for which a relatively large entropic loss (−2.65 kcal/mol) is compensated by a significant enthalpic change (−13.64 kcal/mol), thus presenting the highest affinity in the series (ΔG = −11.0 kcal/mol). Substituting the carbon atom at position 4 following the glycosidic *O*-linkage of HM by sulfur (compound **1**) reduces the Gibbs free energy change from −13.64 to −11.34 kcal/mol. This is partially compensated by a more favorable entropy contribution. The thioalkyl conformation is such that it is positioned between the two tyrosines (Figure S2 of the Supporting Information, **1**). However, the sulfur is turned away from Tyr48 and is in a position where it can stack with the aromatic ring of the more distant Tyr137. The separation of the sulfur atom from Tyr48 and the increased entropy compared to that of HM are probably related to electrostatic repulsion by sulfur.

Calorimetric parameters have been measured at least twice to check for congruency. The best fit is reported together with the standard deviations of the measured values. Compounds are ordered from high to low affinity and grouped into alkyl and aryl mannopyrannosides, respectively.

Also, alkyl mannosides **2** and **3** have very similar enthalpy and entropy changes for FimH binding (Table 1). As HM, they each have an aliphatic chain, but in addition a methyl ester or carboxylate at the distal end (Chart 1). These ligands were synthesized to allow eventual polar interactions, for example, with Thr51, Arg98, or Glu50. However, the introduction of these polar groups reduced the binding enthalpy and enhanced the entropy relative to that of HM, indicating a worse fit in the tyrosine gate.

Within the class of mannopyranosides with aryl moieties in the aglycon, compound **4** (ΔG = −10.55 kcal/mol, and K_d = 18.3 nM) was found to be the better FimH binder (Table 1). Compounds **6** (ΔG = −9.43 kcal/mol, and K_d = 104.6 nM) and **7** (ΔG = −9.50 kcal/mol, and K_d = 94.3 nM), exhibiting the reverse order of the aromatic system and the propargyl group compared with compound **4**, had the lowest affinities in this series. The spatial arrangement of the two hydrophobic functional groups in the tail thus affects the binding affinity (Chart 1). Despite ligands **6** and **7** having very similar affinities, **7** has a higher entropy term and a lower enthalpy term compared to those of **6** (Table 1). This may be due to the electron-pushing nitrogen atom in the pyridine of **7**, complicating aromatic stacking with the Tyr48 side chain. Just like the repulsive sulfur-containing ligand **1**, the aglycon of **7** separates from Tyr48 and moves close to Tyr137. The nitrogen in the pyridine ring makes a strong hydrogen bond with the hydroxyl of Tyr137 in both cocrystals [bond length of 2.8 Å (Figure 2a)] and trigonal crystals soaked with **7** (Figure S2 of the Supporting Information). In contrast, the electron-neutral methoxy group of ligand **6** is too far from the Tyr137 hydroxyl to make a hydrogen bond (Figure 3b). This lack of polar interactions alongside hydrophobic interactions may help explain why the B_{norm} of the aglycon of **6** is the highest of those of all soaked ligands. Nevertheless, the alkyne and aromatic stacking interactions of **6** within the tyrosine gate still contribute significantly to the binding.

Mannopyranosides **4** and **5** show similar ΔG values. The aglycon of both ligands is connected through a phenyl ring to the anomeric center forming the glycosidic *O*-linkage. Nevertheless, the thermodynamic signatures of **4** and **5** are different: ligand **4** makes a smaller enthalpic contribution but gains affinity by a more favorable entropy change. Remarkably, Tyr48 in the complex with ligand **4** occurs in two distinct conformers. The B_{norm} values of Tyr48 and Tyr137 in complex with **4** and **5** are the highest of those of all soaked ligands (Figure 3c), and their aglycons display considerable dynamics and disorder in the electron density maps (Figure S2 of the Supporting Information, **4** and **5**).

DISCUSSION

An initial and crucial step in the pathogenesis of UPEC causing UTIs is mediated by the binding of type 1 piliated bacteria to high-mannose structures present on the uroepithelium.[1,2,5,8] Carbohydrate-based receptor analogues can antagonize the molecular interactions between the FimH adhesin and mannoglycoprotein receptors, thus preventing bacterial adhesion and internalization.[10,9,14,15]

In this work, we determined the three-dimensional structure of the ligand-free FimH LD using X-ray crystallography and analyzed the structures and thermodynamics of complexes of the FimH LD with mannopyranoside derivatives. The ligands exhibited well-defined electron densities in the crystal structures, with full occupancies for the α-D-mannopyranose moieties but with varying degrees of disorder in the aglycons. The crystal structures further demonstrated that the side chain positions of the residues building the mannopyranose-binding pocket, cavity 1, are stabilized upon binding of the receptor. The side chains in cavities 2 and 3 display considerably higher dynamics between crystal structures. In particular, the side chain of Tyr48 was observed in three different rotamers, creating an open, half-open, or closed tyrosine gate together with Tyr137, a gate toward the small, polar mannose-binding pocket.[10,11,27] In the structure bound to the oligomannoside-3 receptor, Tyr48 is in its open conformation and encloses the Man3 and GlcNAc2 pyranose rings in oligomannose-3 (Figure 1a,b).[10] In the previously reported structure of FimH bound to α-D-mannopyranose[27] and in our structure of apo FimH, Tyr48 is also found in its open conformation. This suggests that the open conformation of Tyr48, which leaves the gate "open" toward the mannose-binding pocket for the incoming mannoside, is the minimal energy conformer of the FimH binding site.

Crystal structures of FimH bound to butyl α-D-mannopyranoside (PDB entry 1UWF)[11] and a biphenyl α-D-mannopyranose derivative[13] have revealed that synthetic mannoside derivatives can stabilize alternative conformations of the Tyr48 side chain. Also, the cocrystal structures of mannoside derivatives **7** and **8** reported in this study show that the Tyr48 moves away from its open, resting state. However, it remained unclear whether the different side chain conformations of Tyr48 observed in our cocrystal structures were selected on the basis of favorable dispersion interactions with the apolar aglycons or if they were conformers stabilized by the particular crystal packing.

Consequently, ligands **1**−**8** have been soaked in trigonal apo FimH crystals, where the residues of the receptor-binding site and the tyrosine gate are not constrained by lattice contacts. Electron density maps and atomic displacement parameters of these soaked crystal structures revealed that the side chain of Tyr48 either loses (Oligo-3, **1** and **7**), maintains (**2** and **6**), or gains (**4** and **5**) dynamics upon binding (Figure 3c). The soaked crystal structures also revealed that the presence of an apolar aglycon may challenge Tyr48 from its open

conformation, but it does not favor discrete conformers as might be suggested by cocrystal structures with compounds **7** and **8**. The only exception is ligand **4** that selects two discrete conformers of Tyr48 in monomer A (Figure S2 of the Supporting Information, **4**). Nevertheless, in the FimH crystals soaked with ligands **1**, **2**, and **4**−**7**, the electron density maps were found to show that the aglycon moieties are always seen threading between the two tyrosines of the gate (Figure S2 of the Supporting Information). This sandwiching of the aglycon through the tyrosine gate appears to be a well energy-minimized way of binding and is also seen for the large biphenyl ligand **8** (Figure 2b). The sandwich binding is quite different from binding from this in the $P2_12_12_1$ space group, like for the FimH−**7** complex (Figure 2a), where the pyridine aglycon appears to lie atop a hydrophobic platform formed by the two tyrosines, or to the outdocking mode found for the biphenyl ligand in a cocrystal with the FimH LD.[13]

Following the structural characterizations of FimH complexes with mannopyranosides having alkyl and aryl moieties in the aglycon inhibitor complexes, we wanted to investigate if the degree of dynamics in the FimH−inhibitor complexes is correlated with affinity in terms of entropic contributions to binding. Our ITC measurements indicate that binding of all tested ligands is predominantly enthalpy driven. It is noteworthy that, for this set of ligands, the introduction of an alkyl- or aryl-containing aglycon at the α-anomeric position of D-mannose shifts the entropic factor to a favorable contribution (Figure 4). The release of ordered water molecules into the bulk solvent upon interaction of the hydrophobic surfaces of the aglycon with the FimH tyrosine gate could provide a driving force for hydrophobic interactions,[29,30] to a degree sufficient to compensate for the entropic loss caused by decreased levels of conformational and rotational freedom in the alkyl and aryl ligands upon binding. Remarkably, certain aglycons appear to be unsuitable for stabilizing a discrete Tyr48 rotamer through interaction. This is, for example, demonstrated by ligand **7**, where the Tyr48 side chain is as dynamic in the soaked crystals as in the apo FimH crystals (Figure 3c), thus differing from cocrystals with **7** (Figure 2a) where the aglycon−Tyr48 interactions are stabilized in lattice contacts. Ligands **5** and **6** take this a step further and introduce dynamic disorder into the binding site.

The thermodynamic signatures of FimH with **1**−**3** clearly show a reduced enthalpic change and an enhanced entropy relative to that of HM. These differences are caused by introducing polar groups at the distal end of the alkyl chain or by replacing the aglycon of HM with a thioalkyl chain. The introduction of a hydrophilic group at the end of the aglycon weakens the interactions of the alkyl chain with the FimH binding cavity and results in an increased B_{norm} of ligand **2** from the fifth carbon after the glycosidic *O*-linkage (Figure S2 of the Supporting Information, **2**). The introduction of a methyl ester group at the distal end of a biaryl aglycon was reported to increase affinity, through the ability to form an additional hydrogen bond with the Arg98−Glu50 salt bridge, with the ligand bound in the out-docking mode.[13] In contrast, the structural data for ligand **2** bound to FimH reported here reveal that the methyl esther or carboxyl group of **2** or **3** is not able to form a similar interaction, because the alkyl travels through the tyrosine gate to position its polar end near the hydroxyl of Tyr137, although the distance is too great for formation of a hydrogen bond.

There is an increase in the entropic contribution with alkyl chain length, from mannopyranoside (Man) over methyl α-D-mannopyranoside (MM) to butyl α-D-mannopyranoside (BM). Surprisingly, HM pays a large entropy cost, compensated by the same gain in enthalpy seen for Man. The increased entropic cost of binding of HM on FimH compared to BM might suggest that the heptyl chain makes further contacts with the hydrophobic groove, more than five carbon atoms from the glycosidic linkage as compared to ligand **2**. While it takes on a shape compatible and complementary to that of the tyrosine gate, the alkyl would lose a substantial amount of conformational freedom and thus entropy. Interestingly, the large enthalpy changes of binding of Man and HM are equivalent. Binding of Man to FimH suffers from a huge entropy cost for desolvation. The impact of the release of water molecules upon Man binding can be understood from the crystal structure of apo FimH. Alkylation of Man greatly reduces the loss of entropy through desolvation of Man but at the same time diminishes the enthalpic contribution through solvent reorganization upon the binding of the hydrophobic alkyls.[30] Structural data of FimH−HM complexes would allow further interpretation of these thermodynamic data, especially for the appreciation of possible extended interactions between the FimH tyrosine gate and HM.

In addition to the data for alkyl mannopyranosides given above, we also obtained the thermodynamic signatures for mannopyranosides **4**−**8** with aryl groups in the noncarbohydrate tail. Comparisons of ligand affinities demonstrate that FimH favors a phenyl ring (ligand **4**) over a triple bond (ligands **6**−**8**) to occupy cavity 2 of its receptor-binding site. The preference of FimH for a phenyl ring in cavity 2 is also supported by the high affinities of ligand **5** and of the previously reported tetramer of **4**.[31] The preference for a phenyl ring in cavity 2 is also supported by the high affinity of ligand **5**. In ligands **4** and **5**, the phenyl ring coupled to the glycosidic position has the role of replacing the Man3 pyranoside in the natural FimH receptor oligomannose-3 (Figure 1a,b). However, unlike the pyranoside in the natural ligand oligomannose-3, the phenyl ring in **4** or **5** disturbs Tyr48 in its open conformation (Figure S2 of the Supporting Information, **4** and **5**). This is due to the different angle of the phenyl ring, compared to that of the Man3 pyranose, at the sp^2 chiral center. It can be suggested therefore that a cyclohexane would establish a tighter contact with Tyr48.

On the basis of our structural and thermodynamic data, the binding of α-D-mannopyranosides with alkyl and aryl groups in the aglycon can induce increased dynamics in the tyrosine gate. The tyrosine gate takes on an enhanced dynamics and nondiscrete positions in the soaked trigonal crystal structures when the aglycon fails to make an optimal fit within the tyrosine gate. The failure of the aglycon to take on a conformation compatible with the tyrosine gate and thus contribute with high enthalpy to the interaction can be due to bulkiness (ligands **4** and **5**) or rigidity (ligands **6**−**8**) just after the glycosidic linkage. Electrostatic repulsion, especially at those atomic positions that are suitable for making a close aromatic stacking interaction with the Tyr48 side chain (ligands **1** and **7**), can also be one of the incompatibilities between the ligand and the tyrosine gate. The two porters, Tyr48 and Tyr137, of the tyrosine gate may thus be regarded as entropic levers that help to alleviate the loss of enthalpy, caused by the loss of favorable stacking interactions, by a positive entropic contribution through the introduction of higher dynamics.

dx.doi.org/10.1021/bi300251r | *Biochemistry* 2012, 51, 4790−4799

Interestingly, it is unknown why this mechanism of introduction of dynamics to allow enthalpy−entropy compensation is applied by the FimH adhesin. FimH can recognize all differently linked α-D-mannosides on *N*-linked high-mannose glycans of glycoprotein receptors, albeit with different affinities.[32] The permitted nonideality of the aglycons is possibly related to FimH's ability to deal with less compatible high-mannose structures and still make bacterial adhesion possible. In conclusion, the interpretation of the combination of thermodynamic data with structural data remains a challenging objective but at the same time readily provides important insights into the profile of the interaction of FimH with receptor analogues. This approach will be useful in the creation of better quantitative models to guide the future design of antiadhesive drugs against recurrent or chronic *E. coli* infections.

■ ASSOCIATED CONTENT

Supporting Information

X-ray data collection and crystal structure refinement for ligand-free (apo, PDB entry 4auu) FimH and for cocrystals with ligands **7** (PDB entry 4av4) and **8** (PDB entry 4av5) (Table S1), X-ray data collection and processing, crystal parameters, and refinement statistics for apo FimH crystals in the trigonal space group that have been soaked with ligands **1** (PDB entry 4avh), **2** (PDB entry 4avi), **4** (PDB entry 4auy), **5** (PDB entry 4avj), **6** (PDB entry 4av0), and **7** (PDB entry 4avk) (Table S2), crystal structures in the trigonal space group of the oligomannoside-3-bound FimH (Oligo-3) that was used for molecular replacement and ligand-free (apo) FimH that was used for soaking in the ligands (Figure S1), positions and dynamics of the aglycons of mannoside derivatives soaked into the binding site of FimH in the trigonal crystals, combined with isothermal microcalorimetric raw data and fits (Figure S2), and ITC raw data and fits for the additional mannosides Man, MM, BM, and HM (Figure S3). This material is available free of charge via the Internet at http://pubs.acs.org.

■ AUTHOR INFORMATION

Corresponding Author

*R.R.: Department of Chemistry, P.O. Box 8888, Succ. Centre-Ville, Montréal (QC), Canada H3C 3P8; telephone, (514) 987-3000, ext. 2546; fax, (514) 987-4054; e-mail, roy.rene@uqam.ca. J.B.: Unité de Glycobiologie Structurale et Fonctionnelle, UMR du CMRS 8576, Bâtiment C9, Avenue Mendeleiev, Université Lille 1, 59 655 Villeneuve d'Ascq, France; telephone, +33 320 33 6347; e-mail, julie.bouckaert@univ-lille1.fr.

Notes

The authors declare no competing financial interest.

■ ACKNOWLEDGMENTS

We acknowledge the CNRS for J.B. and the use of beam time at the Proxima 1 beamline at SOLEIL and at the European Synchrotron Radiation Facility beamlines (ESRF). We thank Remy Loris from MoRe (Brussels, Belgium) for access to the Microcal VP-ITC (Hercules).

■ ABBREVIATIONS

UTIs, urinary tract infections; UPEC, uropathogenic *E. coli*; LD, lectin domain; IBC, intracellular bacterial communities; ITC, isothermal titration calorimetry; B_{norm}, normalized *B* factor; Man, mannopyranose; MM, methyl α-D-mannopyranoside; BM, butyl α-D-mannopyranoside; HM, heptyl α-D-mannopyranoside.

■ REFERENCES

(1) Hannan, T. J., Totsika, M., Mansfield, K. J., Moore, K. H., Schembri, M. A., and Hultgren, S. J. (2012) Host−pathogen checkpoints and population bottlenecks in persistent and intracellular uropathogenic *Escherichia coli* bladder infection. *FEMS Microbiol. Rev. 36*, 616−648.

(2) Ofek, I., Mirelman, D., and Sharon, N. (1977) Adherence of *Escherichia coli* to human mucosal cells mediated by mannose receptors. *Nature 265*, 623−625.

(3) Xie, B., Zhou, G., Chan, S. Y., Shapiro, E., Kong, X. P., Wu, X. R., Sun, T. T., and Costello, C. E. (2006) Distinct glycan structures of uroplakins Ia and Ib: Structural basis for the selective binding of FimH adhesin to uroplakin Ia4. *J. Biol. Chem. 281*, 14644−14653.

(4) Eto, D. S., Jones, T. A., Sundsbak, J. L., and Mulvey, M. A. (2007) Integrin-mediated host cell invasion by type 1-piliated uropathogenic *Escherichia coli*. *PLoS Pathog. 3*, e100.

(5) Anderson, G. G., Palermo, J. J., Schilling, J. D., Roth, R., Heuser, J., and Hultgren, S. J. (2003) Intracellular bacterial biofilm-like pods in urinary tract infections. *Science 301*, 105−107.

(6) Mysorekar, I. U., and Hultgren, S. J. (2006) Mechanisms of uropathogenic *Escherichia coli* persistence and eradication from the urinary tract. *Proc. Natl. Acad. Sci. U.S.A. 103*, 14170−14175.

(7) Russo, T. A., Stapleton, A., Wenderoth, S., Hooton, T. M., and Stamm, W. E. (1995) Chromosomal restriction-fragment-length-polymorphism analysis of *Escherichia coli* strains causing recurrent urinary tract infections in young women. *J. Infect. Dis. 172*, 440−445.

(8) Justice, S. S., Hung, C., Theriot, J. A., Fletcher, D. A., Anderson, G. G., Footer, M. J., and Hultgren, S. J. (2004) Differentiation and developmental pathways of uropathogenic *Escherichia coli* in urinary tract pathogenesis. *Proc. Natl. Acad. Sci. U.S.A. 101*, 1333−1338.

(9) Aronson, M., Medalia, O., Schori, L., Mirelman, D., Sharon, N., and Ofek, I. (1979) Prevention of colonization of the urinary-tract by blocking bacterial adherence with methyl-α-D-mannopyranoside. *Israel J. Med. Sci. 15*, 88.

(10) Wellens, A., Garofalo, C., Nguyen, H., Van Gerven, N., Slattegard, R., Hernalsteens, J. P., Wyns, L., Oscarson, S., De Greve, H., Hultgren, S., and Bouckaert, J. (2008) Intervening with urinary tract infections using anti-adhesives based on the crystal structure of the FimH-oligomannose-3 complex. *PLoS One 3*, e2040.

(11) Bouckaert, J., Berglund, J., Schembri, M., De Genst, E., Cools, L., Wuhrer, M., Hung, C. S., Pinkner, J., Slattegard, R., Zavialov, A., Choudhury, D., Langermann, S., Hultgren, S. J., Wyns, L., Klemm, P., Oscarson, S., Knight, S. D., and De Greve, H. (2005) Receptor binding studies disclose a novel class of high-affinity inhibitors of the *Escherichia coli* FimH adhesin. *Mol. Microbiol. 55*, 441−455.

(12) Firon, N., Ashkenazi, S., Mirelman, D., Ofek, I., and Sharon, N. (1987) Aromatic α-glycosides of mannose are powerful inhibitors of the adherence of type 1 fimbriated *Escherichia coli* to yeast and intestinal cells. *Infect. Immun. 55*, 472−476.

(13) Han, Z., Pinkner, J. S., Ford, B., Obermann, R., Nolan, W., Wildman, S. A., Hobbs, D., Ellenberger, T., Cusumano, C. K., Hultgren, S. J., and Janetka, J. W. (2010) Structure-based drug design and optimization of mannoside bacterial FimH antagonists. *J. Med. Chem. 53*, 4779−4792.

(14) Cusumano, C. K., Pinkner, J. S., Han, Z., Greene, S. E., Ford, B. A., Crowley, J. R., Henderson, J. P., Janetka, J. W., and Hultgren, S. J. (2011) Treatment and prevention of urinary tract infection with orally active FimH inhibitors. *Sci. Transl. Med. 3*, 109ra115.

(15) Jiang, X., Abgottspon, D., Kleeb, S., Rabbani, S., Scharenberg, M., Wittwer, M., Haug, M., Schwardt, O., and Ernst, B. (2012) Antiadhesion therapy for urinary tract infections-A balanced PK/PD profile proved to be key for success. *J. Med. Chem. 55*, 4700−4713.

(16) Velazquez-Campoy, A., and Freire, E. (2006) Isothermal titration calorimetry to determine association constants for high-affinity ligands. *Nat. Protoc. 1*, 186−191.

(17) Bock, K., Meldal, M., Bundle, D. R., Iversen, T., Mario Pinto, B., Garegg, P. J., Kvanstrom, I., Norberg, T., Lindberg, A. A., and Svenson, S. B. (1984) The conformation of *Salmonella* O-antigenic oligosaccharides of serogroups A, B, and D1 inferred from ^{1}H- and ^{13}C-nuclear magnetic resonance spectroscopy. *Carbohydr. Res. 130*, 35−53.
(18) Becker, B., Furneaux, R. H., Reck, F., and Zubkov, O. A. (1999) A simple synthesis of 8-(methoxy carbonyl)octyl 3,6-di-*O*-(α-D-mannopyranosyl)-α-D-mannopyranoside and derivatives and their use in the preparation of neoglycoconjugates. *Carbohydr. Res. 315*, 148−158.
(19) Kabsch, W. (1993) Automatic processing of rotation diffraction data from crystals of initially unknown symmetry and cell constants. *J. Appl. Crystallogr. 26*, 795−800.
(20) Mccoy, A. J. (2007) Solving structures of protein complexes by molecular replacement with Phaser. *Acta Crystallogr. D63*, 32−41.
(21) Murshudov, G. N., Vagin, A. A., and Dodson, E. J. (1997) Refinement of macromolecular structures by the maximum-likelihood method. *Acta Crystallogr. D53*, 240−255.
(22) Emsley, P., and Cowtan, K. (2004) Coot: Model-building tools for molecular graphics. *Acta Crystallogr. D60*, 2126−2132.
(23) Moriarty, N. W., Grosse-Kunstleve, R. W., and Adams, P. D. (2009) Electronic Ligand Builder and Optimization Workbench (eLBOW): A tool for ligand coordinate and restraint generation. *Acta Crystallogr. D65*, 1074−1080.
(24) Adams, P. D., Afonine, P. V., Bunkoczi, G., Chen, V. B., Davis, I. W., Echols, N., Headd, J. J., Hung, L. W., Kapral, G. J., Grosse-Kunstleve, R. W., McCoy, A. J., Moriarty, N. W., Oeffner, R., Read, R. J., Richardson, D. C., Richardson, J. S., Terwilliger, T. C., and Zwart, P. H. (2010) PHENIX: A comprehensive Python-based system for macromolecular structure solution. *Acta Crystallogr. D66*, 213−221.
(25) Smith, D. K., Radivojac, P., Obradovic, Z., Dumker, A. K., and Zhu, G. (2003) Improved amino acid flexibility parameters. *Protein Sci. 12*, 1060−1072.
(26) Schon, A., Madani, N., Smith, A. B., Lalonde, J. M., and Freire, E. (2011) Some binding-related drug properties are dependent on thermodynamic signature. *Chem. Biol. Drug Des. 77*, 161−165.
(27) Hung, C.-S., Bouckaert, J., Hung, D. L., Pinkner, J., Winberg, C., Defusco, A., Auguste, C. G., Strouse, R., Langermann, S., Waksman, G., and Hultgren, S. J. (2002) Structural basis of tropism of *Escherichia coli* to the bladder during urinary tract infection. *Mol. Microbiol. 44*, 903−915.
(28) Bouckaert, J., Hamelryck, T. W., Wyns, L., and Loris, R. (1999) The crystal structures of Man(α1−3)Man(α1-O)Me and Man(α1−6)Man(α1-O)Me in complex with concanavalin A. *J. Biol. Chem. 274*, 29188−29195.
(29) Lemieux, R. U. (1989) The origin of the specificity in the recognition of oligosaccharides by proteins. *Chem. Soc. Rev. 18*, 347−374.
(30) Chervenak, M. C., and Toone, E. J. (1994) A direct measure of the contribution of solvent reorganizaion to the enthalpy of ligand binding. *J. Am. Chem. Soc. 116*, 10533−10539.
(31) Touaibia, M., Wellens, A., Shiao, T. C., Wang, Q., Sirois, S., Bouckaert, J., and Roy, R. (2007) Mannosylated G(0) dendrimers with nanomolar affinities to *Escherichia coli* FimH. *ChemMedChem. 2*, 1190−1201.
(32) Bouckaert, J., Mackenzie, J., de Paz, J. L., Chipwaza, B., Choudhury, D., Zavialov, A., Mannerstedt, K., Anderson, J., Pierard, D., Wyns, L., Seeberger, P. H., Oscarson, S., De Greve, H., and Knight, S. D. (2006) The affinity of the FimH fimbrial adhesin is receptor-driven and quasi-independent of *Escherichia coli* pathotypes. *Mol. Microbiol. 61*, 1556−1568.